

## Extremely scaled high-k/ $\text{In}_{0.53}\text{Ga}_{0.47}\text{As}$ gate stacks with low leakage and low interface trap densities

Varistha Chobpattana, Evgeny Mikheev, Jack Y. Zhang, Thomas E. Mates, and Susanne Stemmer

Citation: *Journal of Applied Physics* **116**, 124104 (2014); doi: 10.1063/1.4896494

View online: <http://dx.doi.org/10.1063/1.4896494>

View Table of Contents: <http://scitation.aip.org/content/aip/journal/jap/116/12?ver=pdfcov>

Published by the [AIP Publishing](#)

---

### Articles you may be interested in

[Scaled  \$\text{ZrO}\_2\$  dielectrics for  \$\text{In}\_{0.53}\text{Ga}\_{0.47}\text{As}\$  gate stacks with low interface trap densities](#)

*Appl. Phys. Lett.* **104**, 182912 (2014); 10.1063/1.4875977

[High-performance self-aligned inversion-channel  \$\text{In}\_{0.53}\text{Ga}\_{0.47}\text{As}\$  metal-oxide-semiconductor field-effect-transistors by in-situ atomic-layer-deposited  \$\text{HfO}\_2\$](#)

*Appl. Phys. Lett.* **103**, 253509 (2013); 10.1063/1.4852975

[An investigation of capacitance-voltage hysteresis in metal/high-k/ \$\text{In}\_{0.53}\text{Ga}\_{0.47}\text{As}\$  metal-oxide-semiconductor capacitors](#)

*J. Appl. Phys.* **114**, 144105 (2013); 10.1063/1.4824066

[\$\text{HfO}\_2\$  dielectrics engineering using low power  \$\text{SF}\_6\$  plasma on  \$\text{InP}\$  and  \$\text{In}\_{0.53}\text{Ga}\_{0.47}\text{As}\$  metal-oxide-semiconductor field-effect-transistors](#)

*Appl. Phys. Lett.* **100**, 243508 (2012); 10.1063/1.4729606

[Realization of high-quality  \$\text{HfO}\_2\$  on  \$\text{In}\_{0.53}\text{Ga}\_{0.47}\text{As}\$  by in-situ atomic-layer-deposition](#)

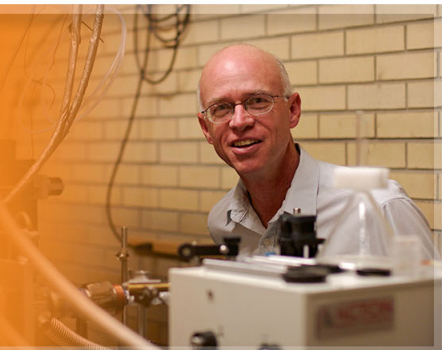
*Appl. Phys. Lett.* **100**, 172110 (2012); 10.1063/1.4706261

---

The logo for AIP Applied Physics Letters features the letters 'AIP' in a large, white, sans-serif font on the left. To its right, the words 'Applied Physics Letters' are written in a smaller, white, sans-serif font, stacked vertically. The background is a dark orange with a subtle, abstract pattern of light-colored, curved lines.

**AIP** | Applied Physics  
Letters

is pleased to announce **Reuben Collins**  
as its new Editor-in-Chief



# Extremely scaled high- $k$ /In<sub>0.53</sub>Ga<sub>0.47</sub>As gate stacks with low leakage and low interface trap densities

Varistha Chobpattana, Evgeny Mikheev, Jack Y. Zhang, Thomas E. Mates, and Susanne Stemmer

Materials Department, University of California, Santa Barbara, California 93106-5050, USA

(Received 1 August 2014; accepted 14 September 2014; published online 24 September 2014)

Highly scaled gate dielectric stacks with low leakage and low interface trap densities are required for complementary metal-oxide-semiconductor technology with III-V semiconductor channels. Here, we show that a novel pre-deposition technique, consisting of alternating cycles of nitrogen plasma and tetrakis(dimethylamino)titanium, allows for HfO<sub>2</sub> and ZrO<sub>2</sub> gate stacks with extremely high accumulation capacitance densities of more than 5  $\mu\text{F}/\text{cm}^2$  at 1 MHz, low leakage current, low frequency dispersion, and low midgap interface trap densities ( $10^{12} \text{cm}^{-2} \text{eV}^{-1}$  range). Using x-ray photoelectron spectroscopy, we show that the interface contains TiO<sub>2</sub> and small quantities of In<sub>2</sub>O<sub>3</sub>, but no detectable Ga- or As-oxides, or As-As bonding. The results allow for insights into the microscopic mechanisms that control leakage and frequency dispersion in high- $k$ /III-V gate stacks.

© 2014 AIP Publishing LLC. [<http://dx.doi.org/10.1063/1.4896494>]

## I. INTRODUCTION

III-V semiconductors have much lower carrier effective masses than Si, which allows for high velocities. They are currently under active investigation to replace Si as the channel in large-scale integrated digital circuits.<sup>1,2</sup> The advantage of a low carrier mass is, however, offset by a low density of conduction band states, which limits achievable carrier densities and thus negatively affects the transistor transconductance. This issue has become known as the “density of states bottleneck.”<sup>3,4</sup> To allow for device scaling to nm-dimensions, gate dielectrics with very high dielectric constants ( $k$ ) are required for large capacitance densities, low tunneling leakage, and to mitigate the density of states bottleneck.<sup>3</sup>

To date, significant efforts have focused on optimizing the interface quality of high- $k$ /III-V interfaces, with remarkable success. For example, the midgap trap densities ( $D_{it}$ ) for gate stacks with high- $k$  HfO<sub>2</sub> and ZrO<sub>2</sub> dielectrics, which can achieve sub-nm equivalent oxide thickness (EOT), are now in the  $10^{12} \text{cm}^{-2} \text{eV}^{-1}$  range.<sup>5–8</sup> Such interfaces allow for excellent transistor performance, including subthreshold slopes of 61 mV/dec and record transconductance.<sup>9,10</sup> Near-ideal subthreshold slopes indicate that the interface is not degraded by interface traps. A common attribute of nearly all high quality high- $k$ /III-V interfaces is the presence of an Al-oxide interface layer, which is either deposited intentionally, or forms during a pre-deposition cleaning process.<sup>5–7,11–13</sup> For example, high-performance HfO<sub>2</sub> and ZrO<sub>2</sub> dielectrics use an *in-situ*, cyclic, pre-deposition tri-methylaluminum (TMA)/nitrogen plasma cleaning process that leads to the formation of a thin Al<sub>2</sub>O<sub>3</sub> layer at the interface.<sup>6,11,14</sup> The presence of Al<sub>2</sub>O<sub>3</sub> severely limits capacitance (or EOT) scaling, because the interface layer is connected in series with the high- $k$  dielectric and Al<sub>2</sub>O<sub>3</sub> has a very low dielectric constant ( $\sim 8$ ). EOT scaling will therefore require either significantly thinning this layer, or replacing it with one that has a higher capacitance density. Furthermore, this must be achieved

without degrading other key properties, in particular, interface trap density and leakage.

TiO<sub>2</sub> has the highest dielectric constant among all binary oxides.<sup>15</sup> Unlike the case for Si,<sup>16</sup> TiO<sub>2</sub> is thermally stable in contact with III-V semiconductors.<sup>17,18</sup> Furthermore, Ti has excellent oxygen gettering properties,<sup>19</sup> which aids in the reduction of native III-V oxides that can be responsible for high  $D_{it}$ .<sup>20–23</sup> Abrupt TiO<sub>2</sub>/In<sub>0.53</sub>Ga<sub>0.47</sub>As interfaces are possible.<sup>17</sup> Here, we report on a method to replace the low- $k$  Al-oxide interface layer with a higher- $k$  Ti-oxide. We show that this can be achieved without degrading the interface quality. In combination with ZrO<sub>2</sub> and HfO<sub>2</sub> dielectrics, Ti-oxide-based interface passivation layers allow for extremely high capacitance densities that exceed the highest reported values by almost a factor of two, while maintaining low  $D_{it}$ . Crystalline TiO<sub>2</sub> has a negligible conduction band offset with In<sub>0.53</sub>Ga<sub>0.47</sub>As, and one may thus predict a large increase in leakage for n-type channels, compared to wide-band gap, Al-oxide based interlayers.<sup>17,24</sup> Contrary to this, we show that gate stacks with Ti-oxide based interface layers show low leakage, similar to what is found for gate stacks with Al<sub>2</sub>O<sub>3</sub> interface layers. Furthermore, the frequency dispersion in accumulation, a known problem of high- $k$ /III-V interfaces,<sup>25</sup> is lower than that of aggressively scaled stacks with Al<sub>2</sub>O<sub>3</sub> interface layers.

## II. EXPERIMENTAL

MOSCAP structures were fabricated on 300-nm-thick,  $n$ -type In<sub>0.53</sub>Ga<sub>0.47</sub>As (Si:  $1 \times 10^{17} \text{cm}^{-3}$ ) epitaxial layers grown by molecular beam epitaxy on (001)  $n^+$ -InP (IntelliEpi, Richardson, Texas). Surfaces were cleaned in buffered HF for 3 min before they were transferred to the atomic layer deposition (ALD) reactor (Oxford Instruments FlexAL ALD). The ALD substrate temperature was set at 300 °C. Samples were heated in hydrogen atmosphere for 3 min. The In<sub>0.53</sub>Ga<sub>0.47</sub>As channel surface preparation was carried out *in-*

*situ* in the ALD system by exposing the surface to cycles consisting of alternating exposures to nitrogen plasma and pulses of tetrakis(dimethylamino)titanium (TDMAT), which is a common ALD precursor for Ti-based layers. This process is very similar to one that uses nitrogen or hydrogen plasma and TMA, reported previously,<sup>6,11,14,26</sup> except that here the TMA was replaced with TDMAT. Each of these cycles consisted of a nitrogen gas set-up step (3 s, 20 mTorr, 20 sccm), a nitrogen plasma pulse (2 s, 20 mTorr, 100 W inductively coupled plasma forward power), a pump step (2 s), a TDMAT dose (500 ms, 200 mTorr, Ar bubbler 100 sccm), a hold step (1 s), followed by purge (3 s) and pump (2 s). The deposition chamber was isolated from the plasma chamber during TDMAT dose to avoid contamination to the plasma chamber. Additional nitrogen plasma and pump steps were added to the end of these cycles. After a fixed number of these cycles, HfO<sub>2</sub> and/or ZrO<sub>2</sub> dielectrics were deposited. The hafnium and zirconium precursors were TEMAHf (tetrakis[ethylmethylamino]hafnium) and TEMAZr (tetrakis[ethylmethylamino]zirconium), respectively. Details of the high-*k* dielectric deposition are described elsewhere.<sup>6,11,14</sup> Variable angle spectroscopic ellipsometry was used to determine the oxide thicknesses on Si pieces, and thickness were also confirmed using STEM. After ALD, plasma-enhanced chemical vapor deposition was used to deposit 500 nm of SiO<sub>2</sub> on the sample backside to protect the InP substrate. The samples were annealed at 400 °C for 15 min in a tube furnace in forming gas (95% N<sub>2</sub> and 5% H<sub>2</sub>). A thermal evaporator was used to deposit metal contacts. 80-nm-thick Ni top contacts ( $7.8 \times 10^{-5}$  cm<sup>2</sup>) were evaporated through a shadow mask. The back Ohmic contact, consisting of Cr (20 nm)/Au (100 nm), was deposited after SiO<sub>2</sub> removal.

Frequency-dependent capacitance-voltage (CV) and conductance-voltage measurements were carried out in the dark from 1 kHz to 1 MHz using an impedance analyzer (Agilent 4294 A). A 300 kV field-emission transmission electron microscope (FEI Titan 80–300) was used for obtaining high-angle annular dark-field scanning transmission electron microscopy (HAADF/STEM) images.

The interface chemistry was investigated using X-ray photoelectron spectroscopy (XPS) (Kratos Axis Ultra DLD). Scans were run using monochromatic Al K $\alpha$  radiation at a pass energy of 20 eV. The energy scales were calibrated by setting the surface aliphatic hydrocarbon peak to 285.0 eV. For quantification, no attempt was made to correct for the fact that layers have different distances to the surface. The relative sensitivity factors used were: Ti 2*p* = 7.8 and In 3*d* = 35 (In 3*d*<sup>5/2</sup> = 21). Scofield's values were modified in some cases by results on standards that can be related back to carbon. For Ti, results on a TiC standard (using high-resolution fits to uniquely identify the carbide peaks) showed that no changes were needed to the Scofield value of 7.8. For In, InN was used, with another standard being used to relate N to C.

### III. RESULTS

Figure 1 shows In 3*d* and Ti 2*p* XPS data for two samples with sufficiently thin (~1 nm) ZrO<sub>2</sub> dielectrics to allow for significant signal from the interface. The ZrO<sub>2</sub> dielectric

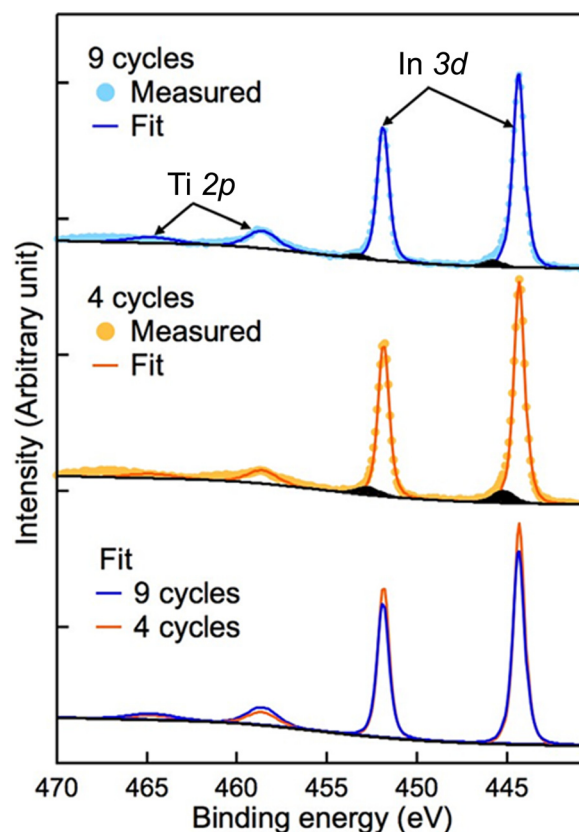


FIG. 1. Ti 2*p* and In 3*d* XPS of ~1 nm ZrO<sub>2</sub>/In<sub>0.53</sub>Ga<sub>0.47</sub>As samples subjected to 9 and 4 cycles of nitrogen plasma/TDMAT pre-treatment. Both samples were annealed in forming gas anneal at 400 °C after ZrO<sub>2</sub> deposition. The black shaded areas indicate peaks associated with In<sub>2</sub>O<sub>3</sub>. The lines are fits to the experimental data.

avoids the issue of Hf peaks overlapping with In, Ga, and As peaks, as is the case for HfO<sub>2</sub>.<sup>6,11</sup> The surfaces were subjected to 9 and 4 nitrogen plasma/TDMAT cycles, respectively, prior to the dielectric ALD. The thin lines are fits to the experimental data. The fits to the In 3*d*<sup>5/2</sup> peaks, at 444.3 eV, are consistent with InGaAs.<sup>27</sup> Because of the overlap with As Auger and In loss signals, Ti 2*p* peaks were extracted by subtracting the signal from an ~1 nm Al<sub>2</sub>O<sub>3</sub>/In<sub>0.53</sub>Ga<sub>0.47</sub>As sample without Ti. This background subtraction removed the low-intensity peaks at 461 and 468 eV, associated with As Auger. The Ti 2*p*<sup>3/2</sup> peaks appear at 458.7 eV, consistent with TiO<sub>2</sub> bonding. We note, however, that sufficient uncertainty exists in the fitting of the Ti peak that it could also be fitted with similar confidence by including an additional set of peaks at 457.1 eV and 463.3 eV, corresponding to Ti<sup>3+</sup>, which could be associated with a suboxide and/or some Ti-N or Ti-O-N bonding. In such a fit, these peaks are about 20% as large as the TiO<sub>2</sub> peaks, therefore possibly equating to something like a monolayer within a 5-atom thick Ti layer. Detecting N directly is difficult in these XPS studies because of the N 1*s*-Ga Auger interference. Comparison of the results for the two samples shows that the sample with 9 cycles of the pretreatment contained a greater amount of Ti than the interface subjected to 4 cycles, as the ratio of Ti:In increases from 0.65 to 0.92. A higher binding energy component (shaded area) of In 3*d*<sup>5/2</sup> is detected at 445.3 eV, indicating the presence of In<sub>2</sub>O<sub>3</sub>.<sup>28</sup>



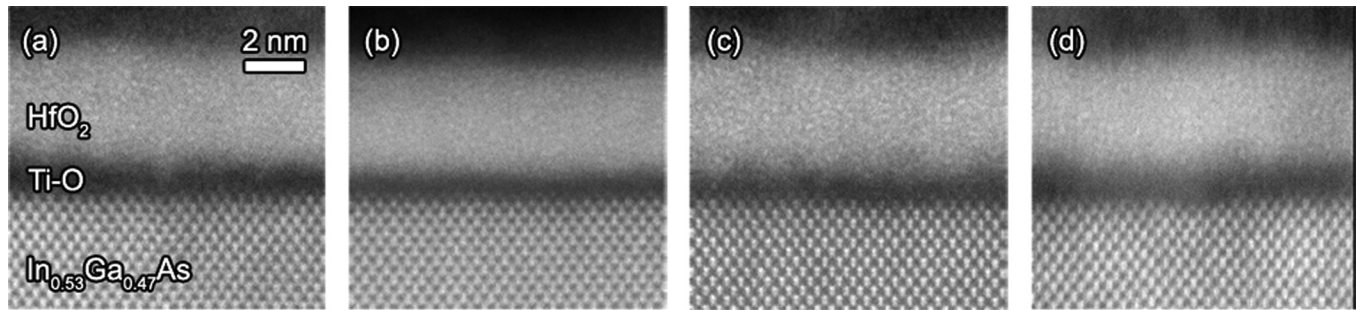


FIG. 2. HAADF/STEM cross-section images of  $\text{HfO}_2/\text{In}_{0.53}\text{Ga}_{0.47}\text{As}$  interfaces, subjected to (a) 9 cycles; (b) 6 cycles; (c) 4 cycles; and (d) 2 cycles of the nitrogen plasma/TDMAT pre-deposition treatment. All samples were annealed in forming gas at  $400^\circ\text{C}$  after  $\text{HfO}_2$  deposition. The TEM foil in (b) is thicker, so the contrast was adjusted for better comparison with the thinner foils.

Quantification from the survey scans (not shown) and the high-resolution peaks suggest that the amount of  $\text{In}_2\text{O}_3$  is approximately 0.3–0.4 at. % of the overall interface region. Considering only the In peak, about 5% of it appeared oxidized, which is likely sufficient to account for an oxidized surface layer (a more accurate estimate is difficult because the XPS signal decreases exponentially as a function of depth, and the oxidized In is closest to the top surface, and therefore disproportionately strong compared to the rest of the In signal). No signatures associated with Ga-oxide, As-oxide, As suboxide, or As-As bonding could be detected. We conclude that the interface layer is mostly  $\text{TiO}_2$  with a small amount of  $\text{In}_2\text{O}_3$  and possibly some nitrogen,<sup>6</sup> and we will refer to it as Ti-O layer in the following.

Figure 2 shows STEM images taken in HAADF mode of four samples with  $\sim 4\text{-nm}$   $\text{HfO}_2$  dielectrics, subjected to the postdeposition anneal at  $400^\circ\text{C}$ . The samples were exposed to different number of cycles (9, 6, 4, and 2, respectively) of nitrogen plasma/TDMAT. A low-atomic-number amorphous layer that is  $\sim 1\text{ nm}$  thick is visible at the interface between  $\text{HfO}_2$  and  $\text{In}_{0.53}\text{Ga}_{0.47}\text{As}$ , and thus likely corresponds to the Ti-O layer detected in XPS (Ti has a lower atomic number than Hf, causing the Ti-O layer to appear dark in HAADF imaging mode). While the  $\text{HfO}_2$  contains small crystallites as a result of the anneal (visible as wormlike contrast in these images), the interface layer remains amorphous, mostly likely due to its small thickness, which affects the crystallization kinetics.<sup>29</sup> The thickness of the amorphous Ti-O layer appears to be relatively independent of the number of pre-deposition cycles. This indicates that its thickness is self-limiting. One explanation is that the first few cycles of the water in the ALD process are the likely to be the source of oxidation. The increase of the interfacial layer thickness is terminated after the high- $k$  layer completely covers the surface. If the thickness of the interfacial layer is approximately constant across the series, one would expect that the capacitance density of the stack increases with increasing number of cycles due to the increase in Ti content detected in XPS (or, alternatively, a reduction in the amount of lower permittivity In-O), which is indeed observed, as described next.

Figure 3 shows frequency-dependent CV characteristics of MOSCAPs from the four different samples for which the STEM images were shown in Fig. 2. The capacitance density in accumulation (large positive gate bias) systematically

increases with the number of pre-deposition cycles, and reaches about  $4.5\ \mu\text{F}/\text{cm}^2$  at 1 MHz for the sample exposed to 9 cycles of nitrogen plasma/TDMAT (Fig. 3(a)). Even higher capacitance densities can be achieved by optimizing the high- $k$  stack. For example,  $\text{HfO}_2/\text{ZrO}_2$  bilayers give excellent results. Figure 4(a) shows the CV characteristics of  $\text{In}_{0.53}\text{Ga}_{0.47}\text{As}$  MOSCAPs with  $\sim 1\text{ nm}$   $\text{HfO}_2/\sim 3\text{ nm}$   $\text{ZrO}_2$  subjected to 6 cycles of the nitrogen plasma/TDMAT pre-treatment. The accumulation capacitance density is  $5.3\ \mu\text{F}/\text{cm}^2$  at 1 MHz and 2 V, almost twice that of other gate stacks reported in the literature, which are less than  $3\ \mu\text{F}/\text{cm}^2$  at 1 MHz.<sup>5–7,14</sup> This sample had an interface layer that was only about 0.5 nm thick (see STEM image in Fig. 4(b)), which is 50% thinner than that of the samples shown in Fig. 3, and contributes to the higher capacitance density. In general, for n-type  $\text{In}_{0.53}\text{Ga}_{0.47}\text{As}$ , the oxide capacitance density ( $C_{\text{OX}}$ ) should be higher than the accumulation capacitance density ( $C_{\text{acc}}$ ), due to the low conduction band density of

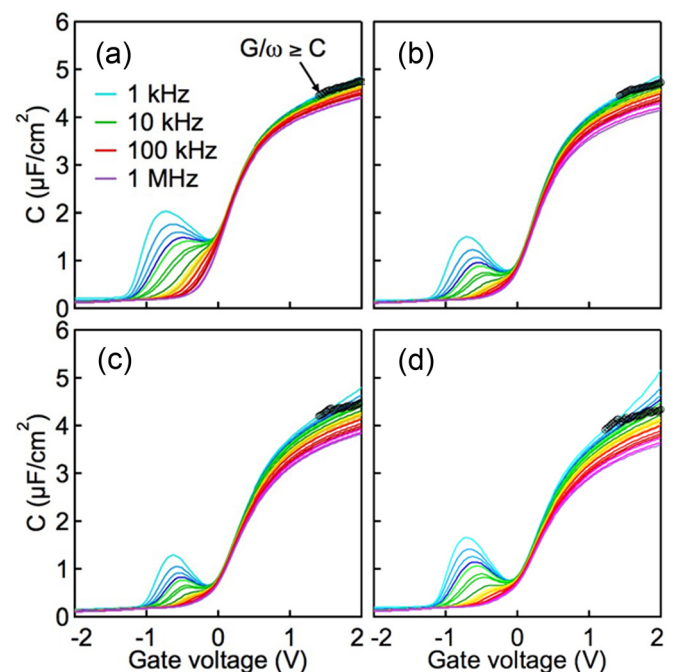


FIG. 3. CV characteristics of  $\text{In}_{0.53}\text{Ga}_{0.47}\text{As}$  MOSCAPs with  $\sim 4\text{ nm}$   $\text{HfO}_2$  subjected to (a) 9 cycles; (b) 6 cycles; (c) 4 cycles; and (d) 2 cycles of nitrogen plasma/TDMAT pre-treatment. The black markers indicate where  $G/\omega \geq C$ .

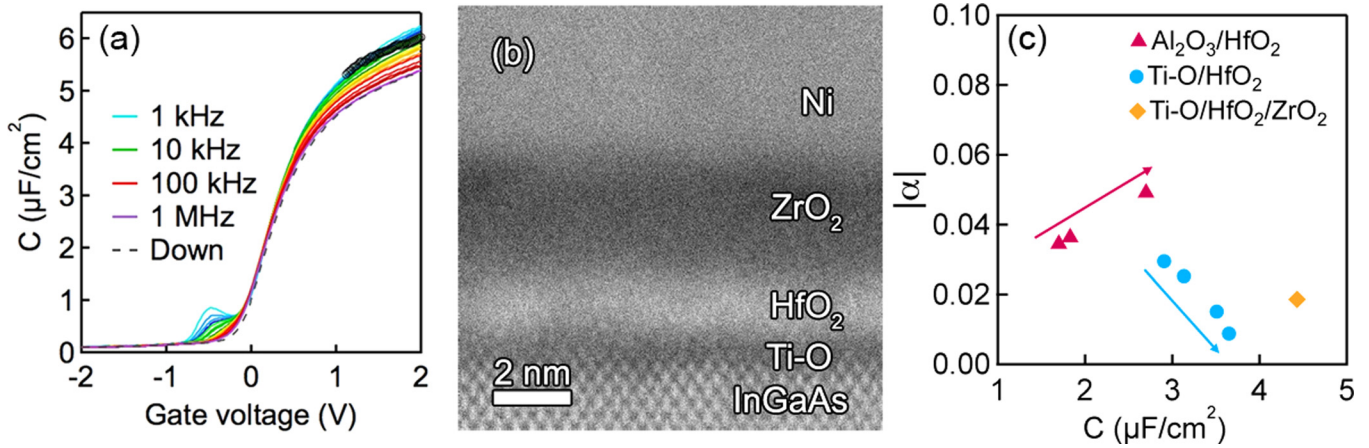


FIG. 4. (a) CV characteristics as a function of frequency and (b) HAADF/STEM cross-section image of  $\text{In}_{0.53}\text{Ga}_{0.47}\text{As}$  MOSCAPs with  $\sim 3$  nm  $\text{ZrO}_2/\sim 1$  nm  $\text{HfO}_2$  subjected to 6 cycles of nitrogen plasma/TDMAT pre-treatment. The dashed line in (a) shows downward (positive to negative voltage) sweep at 1 MHz. The black markers indicate where  $G/\omega \geq C$ . (c) Power law coefficient  $\alpha$  of a power law fit of the frequency dispersion ( $C_{\text{acc}} = Af^\alpha$ ) at +1 V from flatband for  $\text{HfO}_2/\text{In}_{0.53}\text{Ga}_{0.47}\text{As}$  MOSCAPs with nitrogen plasma/TMA pre-treatment, and  $\text{HfO}_2/\text{In}_{0.53}\text{Ga}_{0.47}\text{As}$  and  $\text{ZrO}_2/\text{HfO}_2/\text{In}_{0.53}\text{Ga}_{0.47}\text{As}$  MOSCAPs with nitrogen plasma/TDMAT pre-treatment as a function of the 1 MHz accumulation capacitance density at +1 V from flatband.

states, which adds a semiconductor capacitance in series with the oxide capacitance. The dielectric constant for amorphous  $\text{TiO}_2$  can be as high as 40 (Ref. 30), while the dielectric constants for  $\text{HfO}_2$  and  $\text{ZrO}_2$  depend on their crystalline phase. The dielectric constant of tetragonal  $\text{ZrO}_2$ , which is kinetically stabilized in thin dielectrics,<sup>31</sup> can be as high as 35–50 (Ref. 32).  $\text{HfO}_2$  is typically monoclinic, with a low dielectric constant of about 18. If these three dielectrics are in series,  $C_{\text{OX}}$  of this MOSCAP could approach values of  $6 \mu\text{F}/\text{cm}^2$ , which is higher than the measured  $C_{\text{acc}}$ . While the contribution of the semiconductor capacitance to the accumulation capacitance can, in principle, be calculated,<sup>33</sup> accurate modeling of  $C_{\text{acc}}$  is currently not possible, as discussed below. At low frequencies, the measured accumulation capacitance may also suffer from artifacts from leakage. The black markers in the CV data in Figs. 3 and 4(a) indicate where  $C \geq G/\omega$ , where  $G$  is the measured conductance and  $\omega$  is the frequency. Values above this line are not a measure of the true capacitance density.

The CV characteristics indicate very high quality interfaces. For example, the ideal depletion capacitance value of  $0.119 \mu\text{F}/\text{cm}^2$  is reached, before entering deep depletion, as can be seen from the finite slope at negative gate biases. Deep depletion is one of the best indicators that the Fermi level is unpinned and moves into the lower half of the band gap.<sup>34,35</sup> The CV hysteresis is very small. The dashed line in Fig. 4(a) indicates a hysteresis of  $\sim 0.06$  V around flatband at 1 MHz. By sweeping to a smaller bias range, the hysteresis is reduced. This indicates that charge trapping in the oxide is small. The hysteresis may also have other origins such as generation of minority carriers in the semiconductor, if the CV is swept to high voltages. All CV show a steep slope in the transition to the accumulation. Furthermore, the frequency dispersion at negative biases (hump), which is now well established as being due to midgap  $D_{\text{it}}$  response,<sup>34,36</sup> is small. It increases with increasing number of pre-treatment cycles. Midgap  $D_{\text{it}}$  is typically due to damage (defects) of the semiconductor.<sup>14,37</sup> The results indicate that too many plasma cycles cause damage to the III-V surface.

In addition to the high capacitance density, the samples show remarkably low frequency dispersion in accumulation. All high- $k/\text{In}_{0.53}\text{Ga}_{0.47}\text{As}$  MOSCAPs, with the exception of those that employ a Si interfacial layer,<sup>5</sup> show such frequency dispersion, and its origins are currently debated in the literature.<sup>25,38,39</sup> The frequency dispersion is fairly modest for thick  $\text{Al}_2\text{O}_3$  dielectrics, but increases significantly as the capacitance density is scaled.<sup>40</sup> Figure 4(c) shows a measure of the frequency dispersion in accumulation, expressed in terms of the coefficient  $\alpha$  of a power law fit of the frequency dispersion ( $C_{\text{acc}} = Af^\alpha$ , where  $C_{\text{acc}}$  is the accumulation capacitance density at +1 V from flatband,  $A$  is a constant, and  $f$  is the frequency). Figure 4(c) compares  $\alpha$  for  $\text{HfO}_2$  dielectrics and the bilayer MOSCAP, with  $\text{Al}_2\text{O}_3$  and Ti-O interface layers, respectively, as a function of the maximum capacitance density at 1 MHz. For the  $\text{Al}_2\text{O}_3$  interface layers,  $\alpha$  increases with decreasing  $\text{HfO}_2$  thickness and increasing  $C_{\text{OX}}$ . In contrast, for the Ti-O interface layers, increasing the number of nitrogen plasma/TDMAT cycles (from 2 to 9), results in an increased capacitance density and Ti-content of the interface layer, but decreases the frequency dispersion in accumulation, as can also be seen from Fig. 3. Note that the  $\text{ZrO}_2/\text{HfO}_2$  bilayer stack, which has the highest capacitance density, was exposed to 6 cycles nitrogen plasma/TDMAT, and has a similar  $\alpha$  as the 6 cycle  $\text{HfO}_2$  MOSCAP with nitrogen plasma/TDMAT. We discuss the mechanisms below.

A complete theoretical description of the CV of high- $k/\text{III-V}$  interfaces is still lacking. In particular, at least for n-type channels, the contribution of  $D_{\text{it}}$  to the capacitance in accumulation appears to be non-negligible,<sup>41</sup> even at 1 MHz, due to the fast response of traps near or in the conduction band, as described by

$$\frac{1}{C_{\text{acc}}} = \frac{1}{C_{\text{OX}}} + \frac{1}{C_{\text{Dit}} + C_{\text{S}}}, \quad (1)$$

where  $C_{\text{S}}$  and  $C_{\text{Dit}}$  are the semiconductor and interface state capacitances, respectively. It is believed that the  $D_{\text{it}}$  in the conduction band can be high.<sup>42</sup> This precludes determination

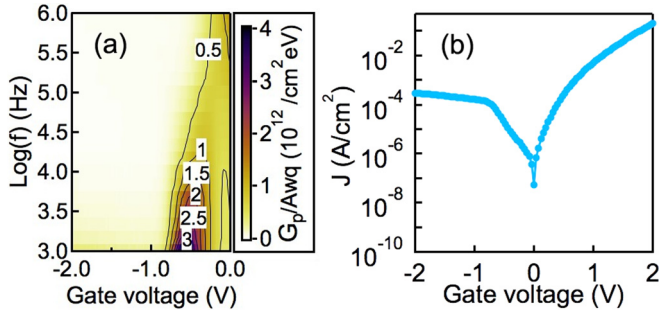


FIG. 5. Conductance map and leakage of  $\text{In}_{0.53}\text{Ga}_{0.47}\text{As}$  MOSCAPs with  $\sim 1$  nm  $\text{HfO}_2/\sim 3$  nm  $\text{ZrO}_2$  subjected to 6 cycles of nitrogen plasma/TDMAT pre-treatment. (a) Normalized parallel conductance maps, showing  $(G_p/A\omega q)_{\max}$  as a function of gate voltage and frequency. (b) Current-voltage characteristics between  $-2$  V and  $2$  V. All measurements are at room temperature.

of the  $D_{it}$  from CV-based methods, which assume that the only contribution of  $D_{it}$  to the high-frequency CV is a stretch-out. Reliable values for the  $D_{it}$  near midgap can be obtained from the conductance method,<sup>34,41</sup> as described next.

To provide a quantitative measure of  $D_{it}$ , Figure 5(a) shows the normalized parallel conductance peak values,  $(G_p/A\omega q)_{\max}$ , where  $G_p$  is the parallel conductance,  $A$  the capacitor area,  $\omega$  the frequency, and  $q$  the elemental charge, as a function of voltage and  $\omega$ , for the sample for which the CV was shown in Fig. 4(a). The  $D_{it}$  can be estimated by multiplying  $(G_p/A\omega q)_{\max}$  with a factor of  $\sim 2.5$ .<sup>43</sup> Near midgap, the  $D_{it}$  values are in the  $10^{12}\text{cm}^{-2}\text{eV}^{-1}$  range, very similar to what is obtained for the best interfaces with Al-O interlayers.<sup>11</sup> Conductance maps also provide a measure of the efficiency of the Fermi level movement in the band gap.<sup>44,45</sup> The  $(G_p/A\omega q)_{\max}$  peak shifts more than two orders of magnitude in frequency as the gate bias is changed between  $-0.25$  and  $-0.75$  V, which indicates a large band bending in response to a change in gate bias.

Figure 5(b) shows the leakage current of the same MOSCAP as a function of gate voltage. The leakage current density is  $5\text{mA}/\text{cm}^2$  at  $1\text{V}$  gate bias, which is below the limit specified by the international technology roadmap for semiconductors. Figure 6(a) shows that the leakage current density barely differs from that of  $\text{HfO}_2$  MOSCAPs with  $\text{Al}_2\text{O}_3$  interface layers and is lower than that of  $\text{ZrO}_2$  MOSCAPs with  $\text{Al}_2\text{O}_3$  interface layers. The leakage is at least an order of magnitude lower than that of other scaled III-V MOSCAPs.<sup>5</sup> As shown in Fig. 6(b), the leakage data are well described by direct tunneling:<sup>46,47</sup>

$$J = \frac{q^3}{16\pi^2\hbar\phi_{\text{OX,eff}}} E^2 \times \exp\left(-\frac{4\sqrt{2m^*}\phi_{\text{OX,eff}}^{3/2}}{3\hbar q} E \left(1 - \left(1 - \frac{V}{\phi_{\text{OX,eff}}}\right)^{3/2}\right)\right), \quad (2)$$

where  $q$ ,  $\hbar$ , and  $E$  are the elementary charge, the reduced Planck's constant, and the electric field, respectively. The fit parameters were the effective barrier height  $\phi_{\text{OX,eff}}$  and the

effective mass  $m^*$ . The image-force-induced barrier lowering was included according to

$$\Delta\phi = \sqrt{\frac{Eq^3}{4\pi\epsilon_0\epsilon_{\text{OX}}}}, \quad (3)$$

where the effective dielectric permittivity,  $\epsilon_{\text{OX}}$ , was estimated to be  $\sim 40$  for amorphous Ti-O and the fitting range was between  $0$  and  $+0.7$  V. As shown in Fig. 6(b) for the sample with  $4\text{nm}$   $\text{HfO}_2$  and  $9$  cycles of pre-treatment, the direct tunneling model describes the leakage data well. Shown in Fig. 6(c) are extracted parameters  $\phi_{\text{OX,eff}}$  and  $m^*$  for the  $\text{HfO}_2$  dielectrics with different number of nitrogen plasma/TDMAT cycles. As the number of cycles increases,  $\phi_{\text{OX,eff}}$  decreases from  $2.06$  to  $1.93$  and  $m^*$  increases from  $0.17$  to  $0.2$ . Since the effects of barrier lowering and the increasing mass offset each other, the leakage current density remains fairly constant. Furthermore, the changes in both parameters are small, and the leakage current density barely differs from that of MOSCAPs with  $\text{Al}_2\text{O}_3$  interface layers (Fig. 6(a)). This is a surprising result, because the conductance band offset between crystalline  $\text{TiO}_2$  and  $\text{In}_{0.53}\text{Ga}_{0.47}\text{As}$  is much smaller than between  $\text{Al}_2\text{O}_3$  and  $\text{In}_{0.53}\text{Ga}_{0.47}\text{As}$  and a much large leakage current density would have been expected. The leakage data suggest that the effective barrier height is close to  $2\text{eV}$ , whereas the conduction band offset between  $\text{TiO}_2$  and  $\text{In}_{0.53}\text{Ga}_{0.47}\text{As}$  is, at most,  $0.6\text{eV}$ .<sup>17,24</sup>

## IV. DISCUSSION

In addition to demonstrating a route to high- $k$ /III-V interfaces with unprecedented high capacitance densities, low leakage, and low  $D_{it}$ , the results shown here are also relevant for several aspects of high- $k$ /III-V interfaces that have been discussed extensively in the literature. The first relates to the origin of the large frequency dispersion that is seen in accumulation, which has been attributed to border traps,<sup>25</sup> near interface traps in the semiconductor,<sup>39,40</sup> and leakage.<sup>38</sup> The precise origins of this frequency dispersion are important because they may negatively affect transistor parameters such as channel mobility or reliability. In general, the frequency dispersion in accumulation increases with the capacitance density, which can be understood from the simple lumped circuit model of the MOSCAP, expressed in Eq. (1): as  $C_{\text{OX}}$  increases, the frequency dispersion caused by  $C_{\text{Dit}}$  increases. Although Eq. (1) refers to the effect of the interface state capacitance,  $C_{\text{Dit}}$ , the lumped circuit models for border traps are basically similar, with the border trap capacitance replacing  $C_{\text{Dit}}$ . It is therefore very important that gate stacks of the same  $C_{\text{OX}}$  are compared when comparing the amount of frequency dispersion.

The results here are contrary to the trend expected from Eq. (1), namely, increasing  $C_{\text{OX}}$  by adding Ti to the interface layer *decreases* the dispersion. In particular, given the high  $C_{\text{OX}}$ , the low frequency dispersion is remarkable. The results show that modifying the chemistry of the interface, in particular replacing the ubiquitously employed Al-O, can lower the frequency dispersion. The results furthermore show that a region very near the interface, confined to no more than the



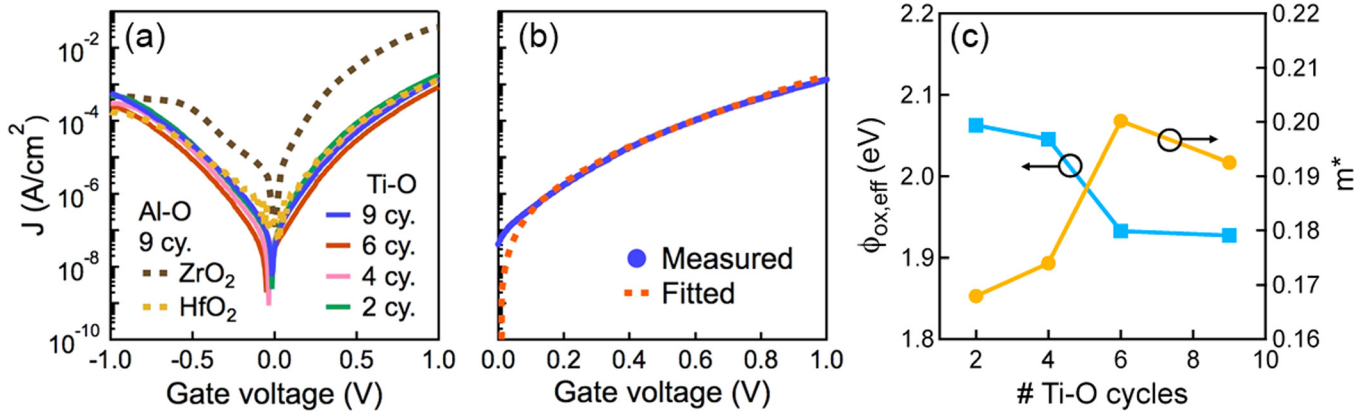


FIG. 6. (a) Current-voltage characteristics of  $\text{In}_{0.53}\text{Ga}_{0.47}\text{As}$  MOSCAPs with either  $\sim 4$  nm  $\text{HfO}_2$  or  $\sim 4$  nm  $\text{ZrO}_2$  dielectrics subjected to 9 cycles of nitrogen plasma/TMA pre-treatment and  $\sim 4$  nm  $\text{HfO}_2$  samples subjected to 9, 6, 4, and 2 cycles of nitrogen plasma/TDMAT pre-treatment. (b) Comparison of measured (solid) and fitted (dashed) current-voltage characteristics between 0 V and 1 V of  $\text{In}_{0.53}\text{Ga}_{0.47}\text{As}$  MOSCAPs with  $\sim 4$  nm  $\text{HfO}_2$  sample subjected to 9 cycles nitrogen plasma/TDMAT pre-treatment. (c) Effective barrier height  $\phi_{\text{ox}}$  and the effective mass  $m^*$  as a function of the number of nitrogen plasma/TDMAT pre-treatment cycles.

thickness of the interfacial layer itself, is key to the microscopic origin of the frequency dispersion. The high- $k$  dielectrics and ALD process are the same in all samples and they should thus contain the same density of defects. This is in keeping with results from modeling of the frequency dispersion.<sup>39</sup> It is interesting to note that the main difference in the chemistry of the interface layers in this study and previously used Al-oxide layers is that Al is replaced with Ti—the amounts of In-oxide are the same as is the lack As-oxides and As-As bonding, at least within the detection limit of XPS. Thus, the study eliminates at least these defects as the origin of large frequency dispersion in accumulation.

The second question relates to what controls the leakage current density in high- $k$ /III-V MOSCAPs. In particular, here, we obtain a counterintuitive result, namely that inserting a low band gap, Ti-O layer at the interface does not change the leakage density from MOSCAPs containing a wide-band gap Al-oxide interface layer. We argue that interface dipoles may largely control the leakage properties of these interfaces. Evidence for such dipoles can be found in shifts in the flat-band voltage ( $V_{\text{FB}}$ ), according to:<sup>48</sup>

$$\frac{V_{\text{FB}}}{q} = \phi_{\text{M}} - \chi_{\text{S}} - \phi_{\text{F}} - \frac{Q_{\text{f}}}{qC_{\text{OX}}} + \phi_{\text{D}}, \quad (4)$$

where  $\phi_{\text{M}}$  is the effective workfunction of the metal,  $\chi_{\text{S}}$  the affinity of the semiconductor,  $\phi_{\text{D}}$  the potential drop due to a dipole layer,  $C_{\text{OX}}$  the oxide capacitance, and  $\phi_{\text{F}}$  is the Fermi energy, given by

$$\phi_{\text{F}} = \frac{E_{\text{g}}}{2} - k_{\text{B}}T \ln\left(\frac{N_{\text{D}}}{n_{\text{i}}}\right), \quad (5)$$

where  $E_{\text{g}}$  the band gap,  $k_{\text{B}}$  is the Boltzmann constant,  $T$  the absolute temperature, and  $N_{\text{D}}$  and  $n_{\text{i}}$  the doping and intrinsic concentrations. In this system,  $\phi_{\text{M}} = 5.15$  eV (Ref. 49),  $\chi_{\text{S}} = 4.5$  eV, and  $\phi_{\text{F}} = 0.06$  eV at 300 K, which gives  $(\phi_{\text{M}} - \chi_{\text{S}} - \phi_{\text{F}}) = 0.59$  eV. The fixed charge at the interface,  $Q_{\text{f}}$ , can be determined from slope of a plot of  $V_{\text{FB}}$  versus thickness,  $t$ , and an estimate for  $\epsilon_{\text{OX}}$ , as shown in

Fig. 7(a). The positive fixed charge density is estimated to be  $1 \times 10^{13} \text{ cm}^{-2}$ , which is about an order of magnitude higher than the fixed charge at the  $\text{HfO}_2/\text{SiO}_2$  interface.<sup>50</sup> The linear dependence of  $V_{\text{FB}}$  on thickness indicates that the influence of oxide fixed charge is small. The intercept, which is smaller than  $(\phi_{\text{M}} - \chi_{\text{S}} - \phi_{\text{F}})$ , indicates the presence of a large *negative* dipole (the positive end of the dipole points to the semiconductor). The extracted dipole

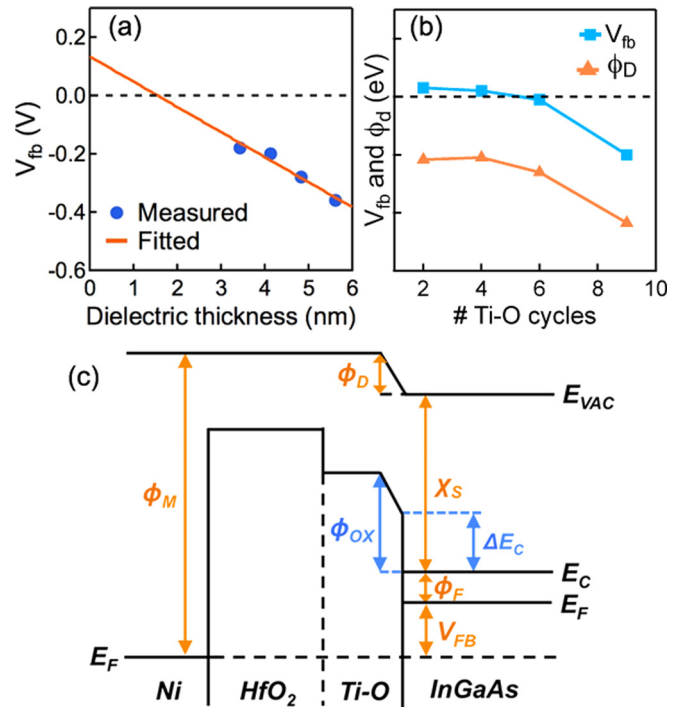


FIG. 7. (a) Flat band voltage as function of  $\text{HfO}_2$  thickness of  $\text{In}_{0.53}\text{Ga}_{0.47}\text{As}$  MOSCAPs subjected to 9 cycles of nitrogen plasma/TDMAT pre-treatment. The line represents a linear fit to the data. (b) Flat band voltage and calculated dipole value as a function of the number of cycles of nitrogen plasma/TDMAT pre-treatment for  $\sim 4$  nm  $\text{HfO}_2/\text{In}_{0.53}\text{Ga}_{0.47}\text{As}$  MOSCAPs. (c) Schematic energy band diagram at flat band of MOSCAP with  $\text{HfO}_2/\text{Ti-O}/\text{In}_{0.53}\text{Ga}_{0.47}\text{As}$  dielectrics showing the effect of an interface dipole on the effective barrier height. The fixed charge is not shown.

values and the flatband voltage for the samples with 2, 4, 6, and 9 cycles of pre-treatment are shown in Fig. 7(b).  $V_{FB}$  shifts to more negative bias as the Ti content in the interface layer is increased, and  $\phi_D$  becomes more negative. A negative dipole serves to increase the effective barrier height,<sup>51,52</sup> as shown in the band diagram in Fig. 7(c). This results in a lower leakage than what would be expected from the band alignments alone. The results in Fig. 6(c), a decreasing band offset by 0.13 eV with increasing Ti content, show that increasingly negative interface dipole does not quite offset the change in band alignments.

## V. CONCLUSIONS

In summary, we have shown that by exposing  $\text{In}_{0.53}\text{Ga}_{0.47}\text{As}$  surfaces to a nitrogen plasma/TDMAT pre-treatment, extremely high capacitance densities can be achieved, through a combination of increasing the permittivity of the interfacial passivation layer with a highly polarizable Ti-oxide, and reducing its thickness to below what is currently possible with the commonly employed Al-oxide interface layers. The extreme increase in capacitance density was achieved without comprising the other key properties, namely  $D_{it}$  and leakage density, which are both similar to those of the best III-V MOSCAPs with Al-oxide interlayers. Similar to previously employed nitrogen plasma/TMA pre-treatments, interfaces are free of Ga-oxides, As-oxides, and As-As bonds, which can be a cause of high  $D_{it}$ .<sup>21–23</sup> Such dielectric stacks should enable extremely scaled III-V transistors for logic devices.

## ACKNOWLEDGMENTS

The authors thank Mark Rodwell for discussions and acknowledge support for this work by the Semiconductor Research Corporation through the Nonclassical CMOS Research Center (Task ID 1437.008). A portion of this work was performed in UCSB's Nanofabrication Facility, which is part of the NSF-funded NNIN network. The work also made use of the MRL Shared Experimental Facilities, which are supported by the MRSEC Program of the NSF under Award No. DMR 1121053.

<sup>1</sup>S. Oktyabrsky, Y. Nishi, S. Koveshnikov, W.-E. Wang, N. Goel, and W. Tsai, in *Fundamentals of III-V Semiconductor MOSFETs*, edited by S. Oktyabrsky and P. Ye (Springer, New York, 2010).

<sup>2</sup>M. Heyns and W. Tsai, *MRS Bull.* **34**, 485 (2009).

<sup>3</sup>M. J. W. Rodwell, U. Singiseti, M. Wistey, G. J. Burek, A. Carter, A. Baraskar, J. Law, B. J. Thibeault, E. J. Kim, B. Shin *et al.*, in 2010 International Conference on Indium Phosphide & Related Materials (IPRM) (2010).

<sup>4</sup>M. V. Fischetti, L. Wang, B. Yu, C. Sachs, P. M. Asbeck, Y. Taur, and M. Rodwell, in IEEE Electron Devices Meeting (IEDM 2007) (IEEE, Washington, DC, 2007), p. 109.

<sup>5</sup>M. El Kazzi, L. Czornomaz, C. Rossel, C. Gerl, D. Caimi, H. Siegwart, J. Fompeyrine, and C. Marchiori, *Appl. Phys. Lett.* **100**, 063505 (2012).

<sup>6</sup>V. Chobpattana, T. E. Mates, W. J. Mitchell, J. Y. Zhang, and S. Stemmer, *J. Appl. Phys.* **114**, 154108 (2013).

<sup>7</sup>R. Suzuki, N. Taoka, M. Yokoyama, S. Lee, S. H. Kim, T. Hoshii, T. Yasuda, W. Jevasuwan, T. Maeda, O. Ichikawa *et al.*, *Appl. Phys. Lett.* **100**, 132906 (2012).

<sup>8</sup>C. W. Cheng, G. Apostolopoulos, and E. A. Fitzgerald, *J. Appl. Phys.* **109**, 023714 (2011).

<sup>9</sup>S. Lee, C. Huang, D. Cohen-Elias, B. J. Thibeault, W. Mitchell, V. Chobpattana, S. Stemmer, A. C. Gossard, and M. J. W. Rodwell, *IEEE Electron Device Lett.* **35**, 621 (2014).

<sup>10</sup>S. Lee, V. Chobpattana, C.-Y. Huang, B. J. Thibeault, W. Mitchell, S. Stemmer, A. C. Gossard, and M. J. W. Rodwell, in *2014 Symposium on VLSI Circuits Digest of Technical Papers* (2014), p. 64.

<sup>11</sup>V. Chobpattana, T. E. Mates, J. Y. Zhang, and S. Stemmer, *Appl. Phys. Lett.* **104**, 182912 (2014).

<sup>12</sup>E. J. Kim, E. Chagarov, J. Cagnon, Y. Yuan, A. C. Kummel, P. M. Asbeck, S. Stemmer, K. C. Saraswat, and P. C. McIntyre, *J. Appl. Phys.* **106**, 124508 (2009).

<sup>13</sup>Y. Xuan, Y. Q. Wu, and P. D. Ye, *IEEE Electron Device Lett.* **29**, 294 (2008).

<sup>14</sup>V. Chobpattana, J. Son, J. J. M. Law, R. Engel-Herbert, C. Y. Huang, and S. Stemmer, *Appl. Phys. Lett.* **102**, 022907 (2013).

<sup>15</sup>R. D. Shannon, *J. Appl. Phys.* **73**, 348 (1993).

<sup>16</sup>K. J. Hubbard and D. G. Schlom, *J. Mater. Res.* **11**, 2757 (1996).

<sup>17</sup>R. Engel-Herbert, Y. Hwang, J. M. LeBeau, Y. Zheng, and S. Stemmer, *Mater. Res. Soc. Symp. Proc.* **1155**, 1155 (2009).

<sup>18</sup>D. G. Schlom, in MRS Fall Meeting, 2008.

<sup>19</sup>H. Kim, P. C. McIntyre, C. O. Chui, K. C. Saraswat, and S. Stemmer, *J. Appl. Phys.* **96**, 3467 (2004).

<sup>20</sup>W. Wang, K. Xiong, R. M. Wallace, and K. Cho, *J. Phys. Chem. C* **114**, 22610 (2010).

<sup>21</sup>L. Lin and J. Robertson, *Appl. Phys. Lett.* **98**, 082903 (2011).

<sup>22</sup>L. Lin and J. Robertson, *J. Vac. Sci. Technol. B* **30**, 04E101 (2012).

<sup>23</sup>H. P. Komsa and A. Pasquarello, *Physica B* **407**, 2833 (2012).

<sup>24</sup>J. Ahn, I. Geppert, M. Gunji, M. Holland, I. Thayne, M. Eizenberg, and P. C. McIntyre, *Appl. Phys. Lett.* **99**, 232902 (2011).

<sup>25</sup>Y. Yuan, L. Q. Wang, B. Yu, B. H. Shin, J. Ahn, P. C. McIntyre, P. M. Asbeck, M. J. W. Rodwell, and Y. Taur, *IEEE Electron Device Lett.* **32**, 485 (2011).

<sup>26</sup>A. D. Carter, W. J. Mitchell, B. J. Thibeault, J. J. M. Law, and M. J. W. Rodwell, *Appl. Phys. Express* **4**, 091102 (2011).

<sup>27</sup>B. V. Crist, *Handbook of Monochromatic XPS Spectra* (Wiley, New York, 2000).

<sup>28</sup>R. J. Hussey, G. I. Sproule, J. P. McCaffrey, and M. J. Graham, *Oxid. Met.* **57**, 427 (2002).

<sup>29</sup>H. C. F. Marten, R. Vlutters, and J. C. Prangma, *J. Appl. Phys.* **95**, 3977 (2004).

<sup>30</sup>V. Mikhelashvili and G. Eisenstein, *Microelectron. Reliab.* **41**, 1057 (2001).

<sup>31</sup>S. Sayan, N. V. Nguyen, J. Ehrstein, T. Emge, E. Garfunkel, M. Croft, X. Y. Zhao, D. Vanderbilt, I. Levin, E. P. Gusev *et al.*, *Appl. Phys. Lett.* **86**, 152902 (2005).

<sup>32</sup>D. Vanderbilt, X. Y. Zhao, and D. Ceresoli, *Thin Solid Films* **486**, 125 (2005).

<sup>33</sup>R. Engel-Herbert, Y. Hwang, and S. Stemmer, *Appl. Phys. Lett.* **97**, 062905 (2010).

<sup>34</sup>R. Engel-Herbert, Y. Hwang, and S. Stemmer, *J. Appl. Phys.* **108**, 124101 (2010).

<sup>35</sup>M. Passlack, M. Hong, E. F. Schubert, G. J. Zydzik, J. P. Mannaerts, W. S. Hobson, and T. D. Harris, *J. Appl. Phys.* **81**, 7647 (1997).

<sup>36</sup>I. Krylov, L. Kornblum, A. Gavrilov, D. Ritter, and M. Eizenberg, *Appl. Phys. Lett.* **100**, 173508 (2012).

<sup>37</sup>G. J. Burek, Y. Hwang, A. D. Carter, V. Chobpattana, J. J. M. Law, W. J. Mitchell, B. Thibeault, S. Stemmer, and M. J. W. Rodwell, *J. Vac. Sci. Technol. B* **29**, 040603 (2011).

<sup>38</sup>A. Ali, H. Madan, S. Koveshnikov, S. Oktyabrsky, R. Kambhampati, T. Heeg, D. Schlom, and S. Datta, *IEEE Trans. Electron Devices* **57**, 742 (2010).

<sup>39</sup>R. V. Galatage, D. M. Zhernokletov, H. Dong, B. Brennan, C. L. Hinkle, R. M. Wallace, and E. M. Vogel, *J. Appl. Phys.* **116**, 014504 (2014).

<sup>40</sup>S. Stemmer, V. Chobpattana, and S. Rajan, *Appl. Phys. Lett.* **100**, 233510 (2012).

<sup>41</sup>H. P. Chen, Y. Yuan, B. Yu, C. S. Chang, C. Wann, and Y. Taur, *Semicond. Sci. Technol.* **28**, 085008 (2013).

<sup>42</sup>N. Taoka, M. Yokoyama, S. H. Kim, R. Suzuki, S. Lee, R. Iida, T. Hoshii, W. Jevasuwan, T. Maeda, T. Yasuda *et al.*, *IEEE Trans. Device Mater. Reliab.* **13**, 456 (2013).

<sup>43</sup>E. H. Nicollian and J. R. Brews, *MOS (Metal Oxide Semiconductor) Physics and Technology* (New York, 1982).

<sup>44</sup>K. Martens, C. O. Chui, G. Brammertz, B. De Jaeger, D. Kuzum, M. Meuris, M. M. Heyns, T. Krishnamohan, K. Saraswat, H. E. Maes *et al.*, *IEEE Trans. Electron Devices* **55**, 547 (2008).



- <sup>45</sup>H. C. Lin, G. Brammertz, K. Martens, G. de Valicourt, L. Negre, W. E. Wang, W. Tsai, M. Meuris, and M. Heyns, *Appl. Phys. Lett.* **94**, 153508 (2009).
- <sup>46</sup>K. F. Schuegraf and C. M. Hu, *IEEE Trans. Electron Devices* **41**, 761 (1994).
- <sup>47</sup>K. Roy, S. Mukhopadhyay, and H. Mahmoodi-Meimand, *Proc. IEEE* **91**, 305 (2003).
- <sup>48</sup>T. W. Hickmott, *J. Appl. Phys.* **51**, 4269 (1980).
- <sup>49</sup>H. B. Michaelson, *J. Appl. Phys.* **48**, 4729 (1977).
- <sup>50</sup>R. Sreenivasan, P. C. McIntyre, H. Kim, and K. C. Saraswat, *Appl. Phys. Lett.* **89**, 112903 (2006).
- <sup>51</sup>J. Hu, K. C. Saraswat, and H. S. P. Wong, *Appl. Phys. Lett.* **99**, 092107 (2011).
- <sup>52</sup>A. P. Huang, X. H. Zheng, Z. S. Xiao, M. Wang, Z. F. Di, and P. K. Chu, *Chin. Sci. Bull.* **57**, 2872 (2012).